Chapter 6

Probing Chemical and Physical Property Changes of Pulmonary Phospholipid Surfactants by Interfacial Ozone Reactions with Field-Induced Droplet Ionization Mass Spectrometry and Microfluidic-Based Bubble Analysis

6.1 Introduction

Lung disease is the third leading cause of death in the United States and lung disease death rates are still increasing.[1] A unique feature of the lungs is that they are constantly exposed to airborne environmental insults. Both short- and long-term exposure of lungs to pathogens, air pollutants, and other irritants can be a major cause of acute distress and contribute to chronic injuries such as cardiopulmonary mortality and lung cancer.[1–3] Recently, Jerret et al. reported a significant increase in the risk of death from respiratory causes in association with air pollution which includes an increase in ozone (O_3) concentration.[4]

Pulmonary surfactant (PS) is a lipid-protein mixture that lines the air-liquid interface of alveolae.[5, 6] The pulmonary surfactant comprises ~ 90% phospholipids and ~ 10% apoproteins by mass.[6] Dipalmitoylphosphatidylcholine (DPPC) is the principal phospholipid component, which achieves very low surface tension (~ 0 mN/m) upon compression.[7, 8] However, it adsorbs and spreads at the air-liquid interface very slowly (0.5

$\mu m^2/s$) at the physiological temperature (37°C), which is below the temperature (T_m) for its gel-to-liquid crystalline phase transition (41°C).[7, 8] Unsaturated phospholipids, owing to their higher fluidity, improve adsorption and spreading properties of surfactant at the air-liquid interface.[8, 9] However, they cannot produce sufficiently low surface tensions when surfactant layers are compressed.[8, 10]

An increasing number of studies have focused on the heterogeneous chemistry of small molecules at the air-liquid interface, mainly using mass spectrometric[11] and spectroscopic[12] techniques, as well as theoretical methods.[13] Recently, real-time monitoring of surface activity of fatty acids has been reported by two research groups.[12, 14] Voss et al. have reported competitive air/liquid interfacial activities involving palmitic acid and oleic acid utilizing broad-bandwidth, sum frequency generation spectroscopy.[12] They observed that a mixed monolayer of the fatty acids was dominated by oleic acid, with palmitic acid becoming predominant when exposure to ozone results in oxidation of the oleic acid to more hydrophilic products. Using a single droplet, Gonzalez-Labrada et al. also reported a decrease in air liquid interface activity of oleic acid after exposure to a monolayer to ozone.[14] Related studies of biologically relevant systems have only just begun, despite their importance. For example, Colussi and co-workers recently reported heterogeneous reactions of O_3 with ascorbic acid[15] and uric acid,[16] which are components of the pulmonary epithelial lining fluid, using ESI mass spectrometry.

Field-induced droplet ionization mass spectrometry (FIDI-MS) comprises a soft ionization method to sample ions from the surface of microliter droplets. FIDI-MS subjects neutral droplets to a strong electric field, leading to formation of dual Taylor cones in which streams of positively and negatively charged submicron droplets are emitted in

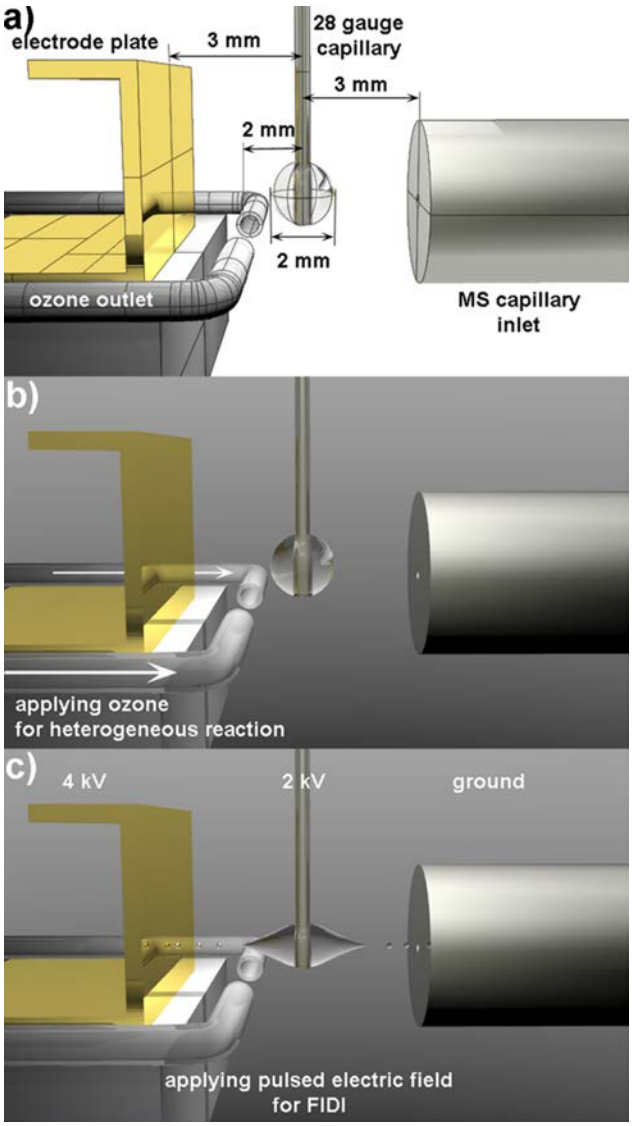

Figure 6.1 (a) Schematic illustration of FIDI-MS setup for heterogeneous reaction study. (b) A quiescent hanging droplet of analyte-containing solution on the end of a capillary is exposed to gas-phase reactants for a variable period of time. (c) After a suitable reaction time, a pulsed electric field stretches neutral droplets until they emit streams of positively and negatively charged submicron droplets in opposite directions. The reactants and product ions of heterogeneous reactions enter the capillary inlet of the mass analyzer.

opposite directions, forming what is essentially a dual electrospray ion source.[11, 17–19] It is ideally suited to monitor time-dependent heterogeneous reactions at the air-liquid interface. Previously, we demonstrated probing time-resolved ozonolysis of oleic acid and oleoyl-L-

α-lysophosphatidic acid using FIDI-MS.[11] In practice, a quiescent hanging droplet is formed on the end of a capillary and then exposed to gas-phase reactants for a variable period of time, followed by FIDI-MS sampling of molecular species present in the interfacial layer (Fig. 6.1).

In this study, we utilize FIDI-MS for probing air-liquid interfacial oxidation by O_3 of 1-palmitoyl-2-oleoyl-*sn*-phosphatidylglycerol (POPG), representative of the major unsaturated anionic lipids in lung surfactant. Sampling droplets with an interfacial layer of POPG exposed to O_3 gas over a range of reaction times reveals the progress of distinct air-liquid interfacial chemistry. The competition of phospholipids subjected to a heterogeneous ozonolysis at the air-liquid interface is also studied using FIDI-MS. A mixture of the saturated phospholipid 1,2-dipalmitoyl-*sn*-phosphatidylglycerol (DPPG) and unsaturated POPG is investigated in negative ion mode using FIDI-MS. A mixture of 1,2-dipalmitoyl-*sn*-phosphatidylcholine (DPPC) and 1-stearoyl-2-oleoyl-*sn*-phosphatidylcholine (SOPC) surfactant is also studied to understand the air-liquid interfacial competition of phospholipids with different polar head groups in positive ion mode. Our results demonstrate that the relatively more hydrophilic products formed by oxidation of the unsaturated phospholipid dissolve back in the aqueous phase, leaving only saturated lipids at the interface. A detailed picture of the interfacial oxidation of unsaturated lipids by O_3 is provided by molecular dynamic (MD) simulations to support our interpretation of the experimental results. Solvation energetics of reactants and products are also evaluated by means of computational modeling. Structures of phospholipids investigated in this study are shown in Scheme 6.1.

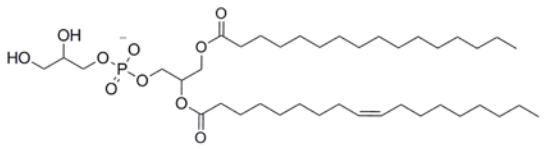

1-Palmitoyl-2-oleoyl-*sn*-phosphatidylglycerol (POPG)

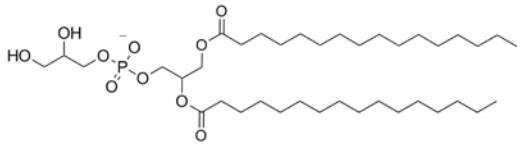

1,2-Dipalmitoyl-*sn*-phosphatidylglycerol (DPPG)

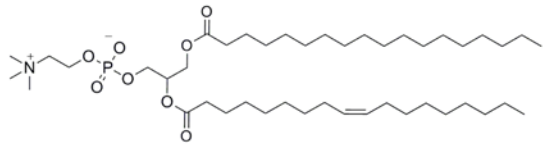

1-Stearoyl-2-oleoyl-*sn*-phosphphatidylcholine (SOPC)

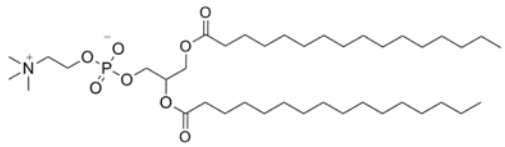

1,2-Dipalmitoyl-*sn*-phosphatidylcholine (DPPC)

Scheme 6.1 Structures of POPG, DPPG, SOPC, and DPPC investigated in this study

Since the chemical modifications in those components will introduce a significant change in the physical characteristics of PS, it is necessary to understand how physical properties at the air-liquid interface will be altered by the chemical changes.

The above-mentioned investigations focused on molecular transformations that occur as a result of oxidative stress. Such molecular transformations can have a strong influence on the physical properties of the PS system (i.e., the surface tension and elasticity of the PS

interface), and so understanding how chemical transformations influence such physical properties can provide key insights into how the PS system responds to environmental challenges. Thus, in the second part of this chapter, we propose to utilize microbubbles as model system for investigating the physical transformations of the PS system when exposed to environmental challenges. Microbubbles have a potential for the interfacial physics study. They have the air-liquid interface and the composition of the interface can be easily modified by utilizing different components in solvent and gas. Interfacial dynamics can be further analyzed in microfluidic systems owing to their small characteristic size and high controllability. [20–23] Especially, the breakup process of bubbles has been intensively studied with various flow parameters and compositions of gas as well as liquid. Prakash et al. showed another feasibility of bubbles in microfluidics by reporting on microfluidic bubble logic.[24] Their results indicate that the bubbles in microfluidic channel can deliver information based on a simplified dynamic flow resistance model. As demonstrated in previous studies, microbubbles in microfluidics impose rich information in their formation process and their behavior in a fluidic channel, which can provide us a comprehensive understanding of the interfacial physics.

In Section 6.3.2, we demonstrate an application of the bubble generation process in microfluidic system to the physical property analysis of lipid surfactant layer at the air-liquid interface as a model of alveolar sacs under oxidative stress condition. As characteristic analysis parameters, size and oscillatory behavior are studied under different conditions: normal air and air with ~ 20 ppm ozone exposures are used. Chemical composition change in a lipid monolayer under ozone exposure is observed by monitoring fluorescence-labeled unsaturated phospolipids at the air-liquid interface. This chemical

composition change, along with physical property change, induces altered bubble size and oscillatory behavior which can provide an improved understanding of the physics of the PS system when it is subjected to oxidative stress.

6.2 Experimental Methods

6.2.1 Chemicals and reagents

Sodium salts of DPPC, DPPG, POPG, SOPC, and NBD-PG (1-oleoyl-2-[12-[(7-nitro-2-1,3-benzoxadiazol-4-yl)amino]dodecanoyl]-sn-glycerol-3-[phospho-rac-(1-glycerol)]) were purchased from Avanti Polar Lipid (Alabaster, AL). All solvents (water and methanol) were purchased from EMD Chemicals, Inc. (Gibbstown, NJ).

6.2.2 Online FIDI-MS technique and heterogeneous oxidation by O_3

The FIDI-MS instrument used in this investigation was based on the design previously described by Grimm et al.[11] An ~ 2 mm o.d. droplet of analyte solution is suspended from the end of a 28 gauge stainless steel capillary (Small Parts, Inc.), which is located between the atmospheric sampling inlet of a Thermo Finnigan LCQ Deca mass spectrometer and a parallel plate electrode. The droplet is centered between the plate electrode and the MS inlet, which are separated by 6 mm. A flow of air containing O_3 is directed at both sides of the droplet by paired ~ 1.6 mm (0.063") id pyrex tubes located 1 mm from the droplet. Ozonolysis reactions occur between 0 and 30 s after a quiescent droplet is achieved (~ 1–2 s). Sampling is affected by pulsed voltages of 4 kV and 2 kV applied to the parallel plate electrode and supporting capillary, respectively. These voltages are tuned to be just above

threshold for initiating FIDI. The high-voltage initiates FIDI and directs submicron-sized charged progeny droplets into the LCQ for mass analysis. POPG and DPPG are monitored in negative ion mode and DPPC and SOPC are monitored in positive ion mode. The FIDI-MS spectra reported in this study were obtained by averaging five to ten individually acquired spectra from separately prepared droplets.

A pencil-style UV calibration lamp (model 6035, Oriel) generates ~ 20 ppm O_3, measured spectrophotometrically using an absorption cell with 10 cm path length and calculated with Beer's Law using the molar absorption coefficient of 1.15×10^{-17} cm^2 $molecule^{-1}$, in air that continually bathes the droplet at 1500 mL min^{-1}. 100 μM POPG or mixtures of 50 μM unsaturated phospholipid (POPG or SOPC) and 50 μM saturated phospholipid (DPPG or DPPC) in 1:1 (by volume) water and methanol feed the droplet source. A recent study of DPPC monolayer on the surface of a water-methanol mixture reported a decrease of the lipid density in the monolayer due to the gradual incorporation of methanol molecules in the monolayer without significant difference of structural and electrical property of the monolayer.[25] In our study, we assume that the structures of the lipid surfactant layers on water-methanol mixtures are similar to their structures on water by itself.

6.2.3 Computational modeling

The MD simulations were performed with the all-atom CHARMM PARAM27 [26] force field using the LAMMPS (Large-scale Atomic/Molecular Massively Parallel Simulator) code.[27] To describe water, we used a flexible TIP3P potential, which incorporates additional Hooke's constants, K, of 900 kcal/mol/$Å^2$ for the OH bond and 110

kcal/mol/rad^2 for the HOH angle to improve the three site rigid TIP3P model.[26] The particle–particle particle–mesh method[28] was employed to compute the electrostatic interactions using an accuracy criterion of 10^{-4}.

The initial structures for the lipid monolayer-water systems were prepared with 48 hexagonally-packed lipids on the 3168, 3264, 3744, and 4464 water molecules for the 55, 60, 65, and 70 Å^2/Lipid surface densities, respectively. A potential of the form, $E = \varepsilon[2/15 (\sigma/r)^9 - (\sigma/r)^3]$, where $\varepsilon = 0.1521$ kcal/mol and $\sigma = 3.1538$ Å with cut-off distance of 2.7071 Å, was applied at z = 0 to prevent water from diffusing in the negative z-direction. The dimensions of the simulation cells used were (55.21 × 47.82 × 200.0 Å) for the 55 Å^2/Lipid, (57.67 × 49.94 × 200.0 Å) for the 60 Å^2/Lipid, (60.02 × 51.98 × 200.0 Å) for the 65 Å^2/Lipid, and (62.28 × 53.94 × 200.0 Å) for the 70 Å^2/Lipid surface densities. The systems were equilibrated for 0.5 ns using 300 K NVT MD simulations by applying Nose-Hoover thermostat with a temperature damping relaxation time of 0.1 ps. Then, 2.0 ns NVT MD simulations were performed, and these trajectories were employed for the analysis of the atomic profiles.

The solvation energy, ΔE_{solv}, of the DPPG, POPG, and oxidative products of POPG (aldehyde and carboxylic acid) were evaluated using the Poisson-Boltzmann model,[29, 30] which is implemented in the Jaguar V 7.5 package (Schrödinger, Inc., Portland, OR). In order to simplify considerations of the effect of functional groups on the solvation energies, analogous extended conformations of all species were employed for the calculations. DFT calculations were performed with the Becke three-parameter functional (B3)[31] combined with the correlation functional of Lee, Yang, and Parr (LYP),[32] using the 6-31G** basis set.

In order to describe the water solvation, solvent probe radius and solvent dielectric constant were set as 1.4 Å and 80.4, respectively.

6.2.4 Design and fabrication of microfluidic device

The microfluidic device was fabricated with PDMS (polydimethylsiloxane, Silgard 184, Dow Chemical, MI, USA) by standard soft lithography.[33] Standard photolithography techniques were utilized to create patterns in SU-8 (MicroChem, MA, USA) photoresist, supported on a Si wafer. The patterned SU-8 film was then used as a mold to cast a PDMS microfluidics chip. The design of the microfluidics was based on a flow focusing device (FFD),[34] combined with a straight microchannel oriented perpendicular to the bubble formation component. The height and width of the main channel was 200 μm, while the height and width of the narrower (bubble generation) channel was 60 μm. Detailed design parameters can be found in Fig. 6.2. The patterned, elastomeric PDMS layer was treated in oxygen plasma, and then bonded to a bare glass slide to form a closed microfluidic channel. Such plasma treatments make the PDMS surface hydropilic and that hydrophilicity was maintained by filling the microchannels with water immediately after the chip was assembled.[34]

6.2.5 Bubble formation tests and analysis

The lipid sample was prepared by mixing 20 μM DPPC and 20 μM POPG in 1×PBS solution. The condition for the bubble generation was optimized for the air condition. The lipid sample flowed at a constant flow rate, 7 μl/min by a syringe pump and either air or ozone was injected at a constant pressure, 0.42 psi. Ozone was generated by a pencil-style

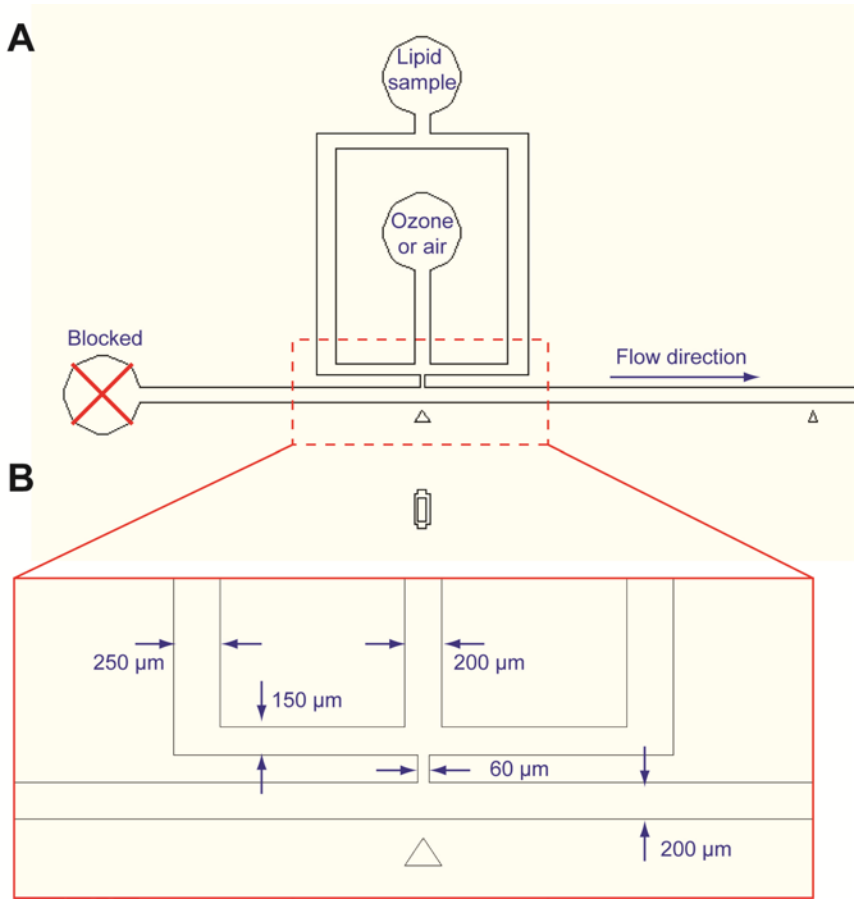

Figure 6.2 Design of the microfluidic device for bubble generation. (A) AutoCAD drawing for the bubble generation component. Either air or ozone is introduced from the center channel and the lipid sample flows in from the outer two channels. Lipid sample flow pinches off the gas to form bubbles. The hole in the left is used to introduce water right after plasma-based bonding for the hydrophilicity of the channel and remains blocked with a pin-plug for the rest of the process. (B) Zoomed-in image of the main components of the bubble formation with dimensions

UV calibration lamp (model 6035, Oriel) that was placed upstream of the pressure regulator. By turning on the UV lamp, air flow was converted to ozone flow. Ozone concentration was measured spectrophotometrically and maintained as 20 ppm.

The bubble formation process was monitored by a microscope throughout the experiments and recorded as a movie at 30 frames/sec by a CCD camera. All the images were extracted from the movie by DVDVideoSoft (DVDVideoSoft.com) and analyzed

with ImageJ (NIH) for the size and the generation time for the bubbles. The formation times for the first thirteen bubbles were measured for the analysis. For the bubble size analysis, the lengths of twenty bubbles were measured and 10% sample trimmed mean was obtained for the analysis.

6.2.6. Analysis and imaging of the ozone effect

To visualize the ozone effect at the interface, fluorescence-labeled PG lipid was added to the lipid sample. The lipid sample composition was 20 μM DPPC, 10 μM POPG, and 10 μM NBD-PG in 1×PBS solution. The same flow condition as for the bubble formation test was used while monitoring the fluorescence. Fluorescence images were taken by a fluorescence confocal microscopy for the air as well as the ozone conditions. 10 frames averaged image with the exposure of 7.2 μs and the gain of 7.7 was taken for visualization. Gray value intensity was measured with ImageJ.

6.3 Results and Discussion

6.3.1 Probing chemical property changes by FIDI

Interfacial Reaction of POPG with O_3. The *cis*-double bond of an unsaturated phospholipid reacts with O_3, yielding aldehyde and carboxylic acid products directly from primary ozonide (POZ) or through energetic Criegee intermediates (CI), while saturated phospholipids such as DPPG and DPPC remain intact. In this study we have investigated the heterogeneous reaction of O_3 with POPG as a representative unsaturated phospholipid in the PS system.

The negative ion FIDI-MS spectra for ozonolysis of POPG in a water/methanol (1:1 by volume) droplet are shown in Figure 6.3. Singly deprotonated POPG, observed at m/z 747, is seen as a dominant species in the FIDI-MS spectrum before O_3 application. Products resulting from ozonolysis of POPG appear at least as early as 5 s after exposing the droplet to O_3. The aldehyde and carboxylic acid products are observed at m/z 637 and m/z 653, respectively. In addition, hydroxyhydroperoxide (HHP), methoxyhydroperoxide (MHP), and what we assume to be the secondary ozonide (SOZ) are also observed as products of POPG ozonolysis at m/z 671, m/z 685, and m/z 795, respectively. The relative abundance of the reactant POPG decreases dramatically after 15 s of exposure, and the FIDI-MS spectrum is dominated by ozonolysis products after 30 s.

The formation of primary ozonide (POZ), which is the first step in the ozonolysis of POPG at the air-liquid interface, is described as

$$O_3 + POPG \xrightarrow{k_1} POZ \quad . \tag{6.1}$$

The ozone concentration is assumed to be constant during the reaction, which allows calculating the reaction rate using the pseudo-first-order rate constant $k_2 = k_1[O_3]$, where $k_1 = 4.5 \times 10^{-16}$ cm^3 $molecule^{-1}$ s^{-1} adopted from ozonolysis of OPPC on NaCl.[35] The applied ozone concentration is ~ 5×10^{14} molecule cm^{-3} (20 ppm). The reaction rate is expressed as

$$-\frac{d[POPG]_{surf}}{dt} = k_2[POPG]_{surf,0} \quad . \tag{6.2}$$

Solving eq. 6.2 gives

$$\frac{[POPG]_{surf}}{[POPG]_{surf,0}} = e^{-k_2 t} \quad . \tag{6.3}$$

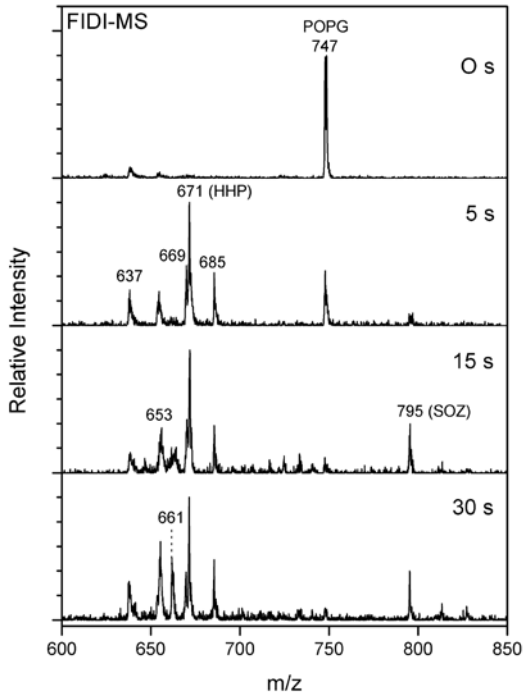

Figure 6.3 Heterogeneous reaction of POPG with O_3 as a function of time. In the absence of ozone, the negative ion FIDI-MS spectrum of POPG is dominated by the singly deprotonated POPG peak at m/z 747. POPG is depleted after 15 s of exposure, and oxidation products are dominated by deprotonated HHP at m/z 671. The aldehyde, carboxylic acid, and methoxyhydroperoxide products are observed at m/z 637, m/z 653, and m/z 685, respectively. The SOZ and sodiated alcohol products show up in the spectra at m/z 795 and m/z 661, respectively. The structure of each product is shown in Scheme 6.2.

For 90% and 99% depletion of POPG at the air-liquid interface, it takes ~ 10 s and ~ 20 s, respectively. This agrees well with the experimental observation of this study.

It is noteworthy that hydroxyhydroperoxide (HHP), methoxyhydroperoxide (MHP), and the SOZ, which are known to be metastable species in the bulk phase, are observed as major products of POPG ozonolysis in the FIDI-MS spectra (Figure 6.3).[35] In order to yield HHP, a Criegee intermediate (CI) or a POZ is required to react with a water molecule.[35, 36] Rapid decomposition of HHP through proton transfers from water molecules yields

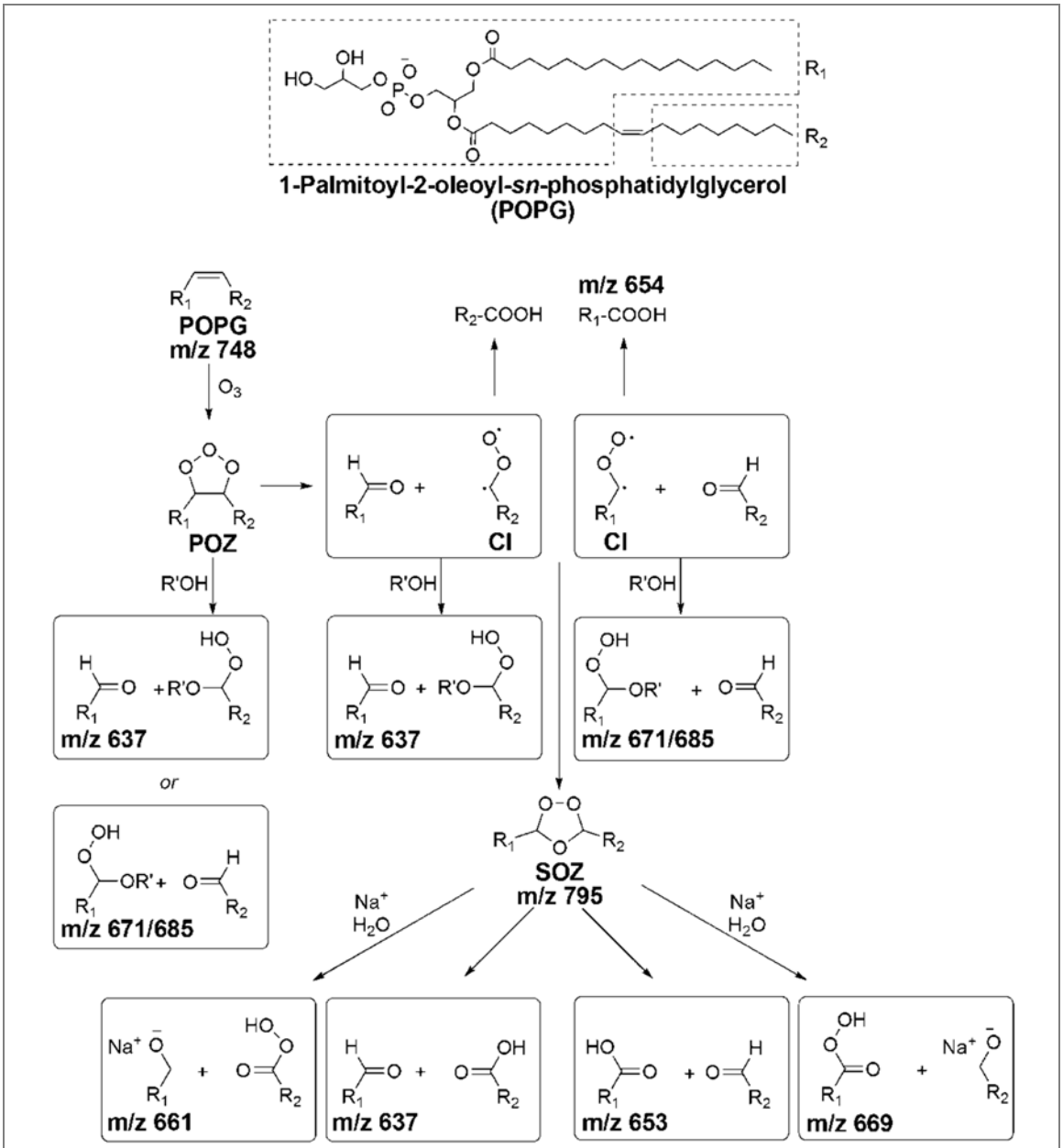

Scheme 6.2 Summary of heterogeneous oxidation of POPG with O_3 at the air-liquid interface. R′ is H for water and CH_3 for methanol.

ROS,[36] which makes it difficult to observe HHP directly in the bulk-phase. The water density at the air-liquid interfacial region is significantly lower than in the bulk-phase.[37] In addition, water molecules in a lipid layer at the air-liquid interface are observed to be localized within the lipid head group region due to the strong interactions with polar head

groups.[38] These conditions allow HHP to be abundant in the lipid layer at the air-liquid interface, which is a characteristic of the heterogeneous reaction of POPG compared to the homogeneous reaction.[36] The observed MHP originates from the reaction of a CI or POZ with a methanol molecule in the droplet. The proposed reaction mechanisms are shown in Scheme 6.2.

A significant abundance of SOZ is observed in the FIDI-MS spectra after exposing the droplet to O_3 for 15 s. The structure of SOZ (m/z 795) is confirmed by low-energy-collision induced dissociation (CID), which yields the aldehyde (m/z 637) and carboxylic acid (m/z 653) fragments (Fig. 6.4). The peak corresponding to SOZ continues to build up

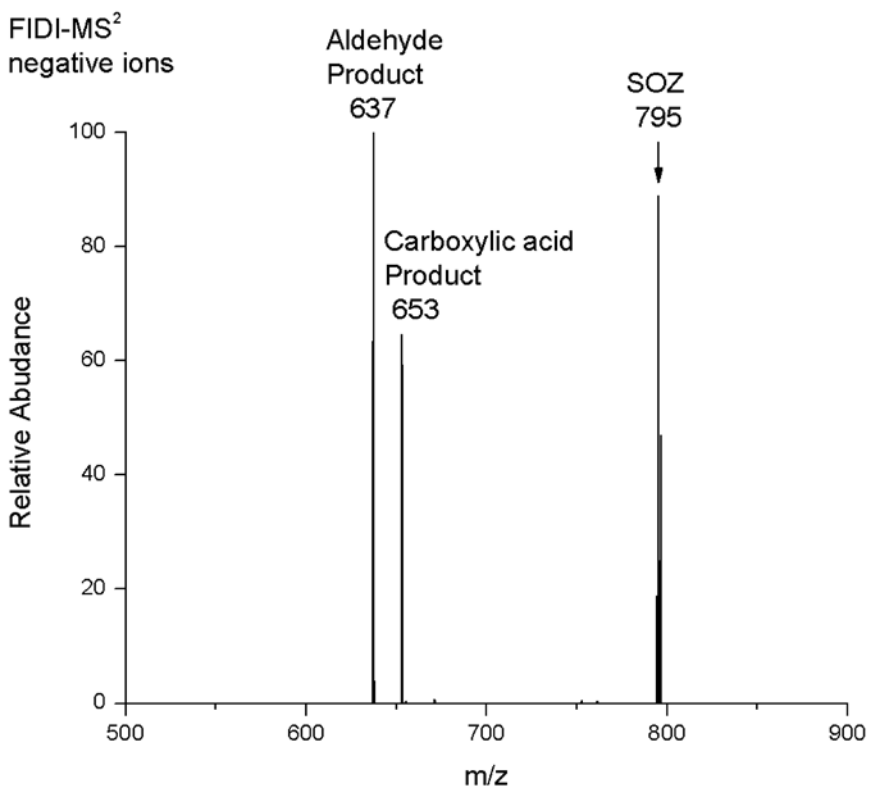

Figure 6.4 The FIDI-MS^2 spectrum of SOZ at m/z 795 showing two competitive products at m/z 637 and at m/z 653, which correspond to the aldehyde and carboxylic acid fragments, respectively

in the spectrum as the POPG lipid is depleted. We infer that the observed SOZ is not formed by direct rearrangement of POZ but rather by recombination of the CI with aldehydes (Scheme 6.2).[35, 39] In the bulk-phase, however, faster reaction with water molecules prevents the CI from reacting with aldehyde to form SOZ.[40] A significant amount of the sodiated alcohol product (m/z 661) is observed after exposing the droplet to O_3 for 30 s. This product is due to the dissociation of SOZ followed by the association with sodium cation. This suggests that after SOZ is produced in an anhydrous environment, the newly formed hydrophilic molecule interacts with sodium cation in the liquid-phase to yield the sodiated alcohol product. These SOZ and sodiated alcohol products are characteristic of specific air-liquid interface chemistry during POPG ozonolysis.

Interfacial Reaction of a POPG and DPPG Mixture with O_3. Figure 6.5 shows negative ion FIDI-MS spectra for the heterogeneous ozonolysis at several reaction times of a mixture of DPPG and POPG at the air-liquid interface. Conditions employed are identical to those used to obtain the data shown in Figure 6.3. Singly deprotonated DPPG and POPG, observed at m/z 721 and m/z 747, respectively, dominate the FIDI-MS spectrum before O_3 application, suggesting that the pulmonary surfactants DPPG and POPG form a mixed interfacial layer. The products resulting from the ozonolysis of POPG appear at least as early as 5 s after exposing the droplet to O_3. All products, including aldehyde (m/z 637), carboxylic acid (m/z 653), HHP (m/z 671), and MHP (m/z 685), are observed to result from ozonolysis of POPG in the mixed surfactant system. The relative abundance of the reactant POPG decreases by half after 15 s of exposure, while the product abundance continues to increase after up to 30 s of exposure. The FIDI-MS spectrum is dominated by DPPG after 45 s.

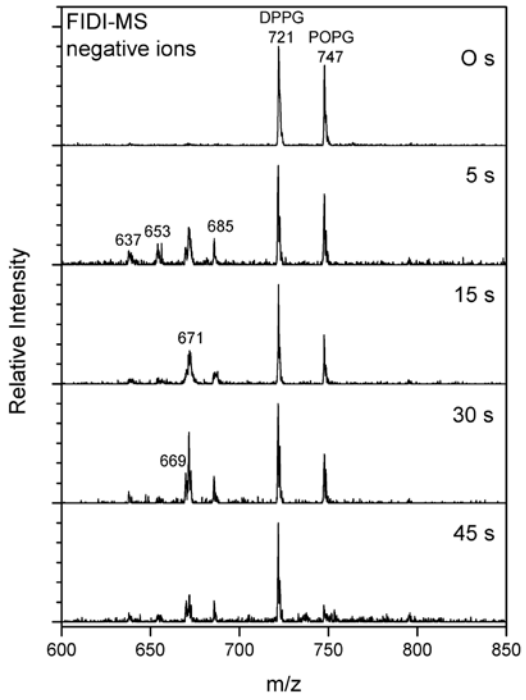

Figure 6.5 Heterogeneous reaction of a 1:1 mixture of POPG and DPPG with O_3 as a function of time. In the absence of ozone, the negative ion FIDI-MS spectrum is dominated by singly deprotonated POPG and DPPG at m/z 747 and m/z 721, respectively. The oxidation products of POPG—including aldehyde (m/z 637), carboxylic acid (m/z 653), HHP (m/z 671), and MHP (m/z 685)—are observed after 5 s of O_3 exposure. Singly deprotonated DPPG dominates the FIDI-MS spectrum after 45 s.

The absence of any ozonolysis products from the saturated lipid DPPG indicates that only the unsaturated lipid POPG reacts with ozone. Several differences are observed from the heterogeneous ozonolysis of the DPPG and POPG mixture compared to the ozonolysis of POPG alone. First, with extensive ozonolysis, the products disappear from the surface of the droplet, leaving only DPPG at the interface. The ozonolysis products of POPG are expected to be more hydrophilic than the precursor (Scheme 6.2). The data in Fig. 6.5 suggest that these hydrophilic products diffuse into the aqueous droplet, leaving only hydrophobic DPPG in the interfacial surfactant layer. Comparison of the results in Figs. 6.3

and 6.5 indicate that the overall ozonolysis reaction of POPG, including the depletion of POPG on the surface of the droplet, is slower in a mixture with DPPG.

The lipid tails of DPPG adopt a highly ordered arrangement in a surfactant monolayer.[41] In the mixture of a DPPG and POPG, the saturated acyl chains of DPPG may act to shield POPG, limiting the approach of O_3 to the unsaturated carbons of POPG, with a corresponding slower reaction compared to POPG alone. Note also that a significant abundance of SOZ is not observed in the FIDI-MS spectrum of a mixture of DPPG and POPG (Fig. 6.5). As discussed earlier, SOZ is formed by the recombination of the CI with aldehyde under an anhydrous environment (Scheme 6.2).[35, 39] In the mixed surfactant layer, competition on the droplet surface is expected between hydrophobic DPPG and the relatively hydrophilic nascent products of POPG ozonolysis. This accounts for the observed predominance of DPPG in the FIDI-MS data at long times.

Interfacial Reaction of a SOPC and DPPC Mixture with O_3. We also investigated the heterogeneous reaction of O_3 with a mixture of saturated and unsaturated lipids using SOPC and DPPC in the positive ion mode (Fig. 6.6). In contrast to phosphatidylglycerol (PG), the positive ion mode FIDI-MS spectra of phosphatidylcholine (PC) show additional dimeric complexes along with monomers as sodiated species. The sodiated DPPC and SOPC monomers are observed at m/z 756 and m/z 810, respectively. The sodiated complexes at m/z 1489 and m/z 1597 are DPPC dimer and SOPC dimer, respectively. The heterogeneous dimeric complex of DPPC and SOPC is observed at m/z 1543. The measured intensity of the homogeneous and heterogeneous dimeric complexes are not very different from the statistical ratio (1:2:1) indicating that DPPC and SOPC form a well-mixed interfacial layer. The FIDI-MS spectrum reveals the ozonolysis products after 5 s of

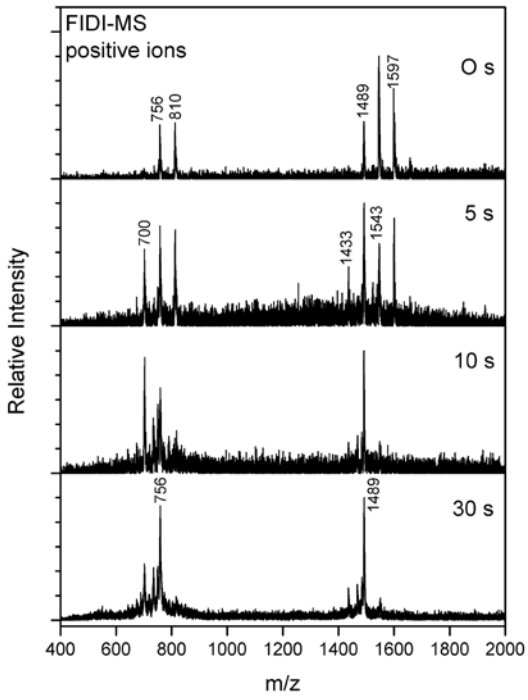

Figure 6.6 Heterogeneous reaction of a 1:1 mixture of SOPC and DPPC with O_3 as a function of time. In the absence of ozone, the positive ion FIDI-MS spectrum shows the singly charged sodiated DPPC and SOPC monomoers at m/z 756 and m/z 810, respectively. The singly charged mono-sodiated DPPC and SOPC homodimers are observed at m/z 1489 and m/z 1597, respectively. The singly sodiated heterogeneous dimer of DPPC and SOPC appears at m/z 1543. The oxidation products of SOPC, including monomeric aldehyde product (m/z 700) and the complex of DPPC and aldehyde product (m/z 1433), are observed after 5 s of O_3 exposure. Sodiated DPPC monomers and dimmers of DPPC dominate the FIDI-MS spectrum after 30 s.

O_3 exposure. The product at m/z 700 corresponds to the sodiated aldehyde product of SOPC. The sodiated complex of intact SOPC and the aldehyde product of SOPC are observed at m/z 1543. With extensive ozonolysis (15 s), SOPC is depleted, and eventually the aldehyde products also disappear from the spectrum, suggesting that only DPPC remains in the surfactant layer.

In contrast to the negative FIDI-MS spectra of POPG, only aldehyde products are observed from the ozonolysis of SOPC. The only significant difference between the two

lipids is the nature of the polar head group, which is acidic in the case of the phosphatidylglycerol lipid and amphoteric (zwitterionic) in the case of the phosphatidylcholine lipid. However, it is not obvious how this might influence the observed difference in ozonolysis products. The two mixtures are similar in that at long times the more hydrophilic oxidation products disappear from the spectra as they are dissolved into the aqueous phase.

Note also that depletion of SOPC oxidation products occurs more rapidly from ozonolysis of the mixture of SOPC and DPPC compared to ozonolysis of the POPG and DPPG mixture. In forming a surfactant layer the fatty acid chains of the saturated phospholipid DPPC exhibit less-orderly packing compared to those of DPPG.[41] More random orientation of DPPC fatty acid chains may cover unsaturated carbons of SOPC less effectively compared to DPPG, allowing SOPC to react with ozone more easily.

Water Density at the Position of Unsaturated Carbons in a Lipid Monolayer. As discussed above, the unique low water density environment of the air-liquid interface may allow us to observe metastable HHP and POZ in the heterogeneous ozonolysis of POPG. In order to develop a more detailed picture of the interfacial environmental, we carried out MD simulations for the POPG monolayer in a water box for 2.0 ns with four different surface densities (55, 60, 65, and 70 $Å^2$/lipid). These surface densities are reported as a proper density range for pulmonary surfactant function from previous theoretical studies.[41–43] The final snapshot in Fig. 6.7a shows the POPG monolayer at the air-liquid interface monolayer with 60 $Å^2$/lipid surface density as a representative case. Fig. 6.7b shows the atomic density profiles of oxygen atoms of water molecules, saturated carbon atoms, and unsaturated carbon atoms of lipid acyl chains along $\pm\Delta z$, which is z-direction relative to the

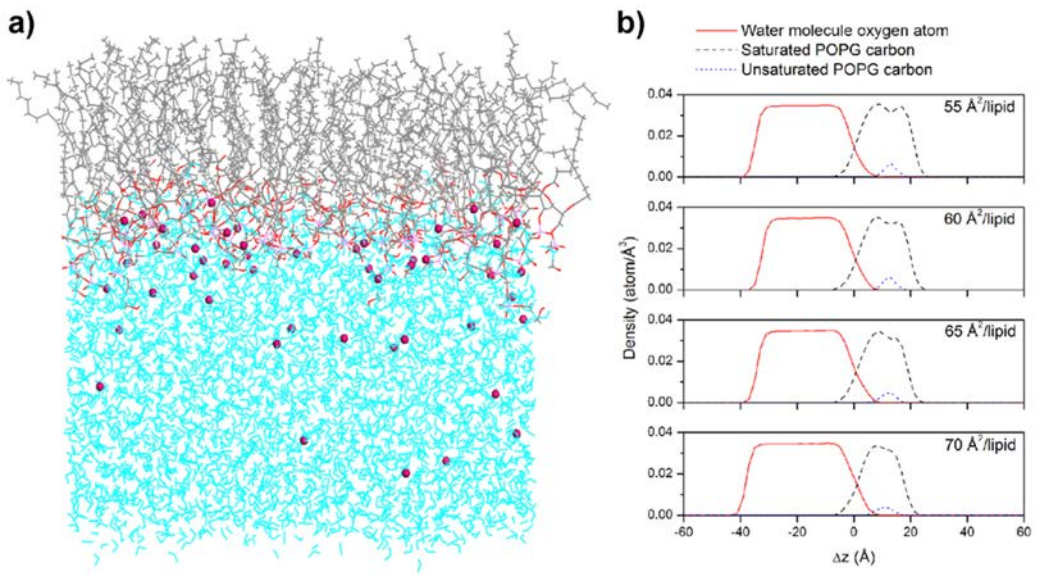

Figure 6.7 (a) Final snapshot after 2.0 ns of MD simulation of a POPG monolayer at 60 $Å^2$/lipid. Water molecules and chloride ions are shown in cyan and purple, respectively. (b) Atomic density profiles of POPG monolayer systems as a function of Δz, where the air/liquid interface is 0 (negative values are toward the water layer, and positive values are toward the lipid). The lipid surface densities are 55 $Å^2$/lipid, 60 $Å^2$/lipid, 65 $Å^2$/lipid, and 70 $Å^2$/lipid. Red solid lines denote that of unsaturated carbons of lipid acyl chains, black dashed lines denote that of saturated carbons of lipid acyl chains, and blue dotted lines denote the density profiles of oxygen atoms of water molecules.

averaged position of the phosphorous atom of POPG. The interaction between POPG and water occurs in the region of overlapping density. The lipid head group is solvated, reflecting the strong ion-dipole interactions between the POPG phosphate group and water molecules. However, the water density at the double bond of POPG (5–20 Å) is ~ 0.0005 atom/$Å^3$, which is ~ 70 times less dense than in the bulk-phase (~ 0.035 atom/$Å^3$) when the POPG monolayer has 60 $Å^2$/lipid surface density. This indicates that a limited number of water molecules are involved when ozone interacts with the double bond of POPG. A single water molecule is required to form a HHP from a CI or a POZ.[35, 36] Further reactions with water molecules result in formation of ROS (Scheme 6.2).[36] The low water

concentrations around the double bond allow HHP to survive sufficiently long to be observed in the FIDI-MS spectra. It is noteworthy that SOZ appears after POPG is depleted on the surface of the droplet (Fig. 6.3). The fast reaction with water inhibits formation of SOZ from CI when water molecules are accessible.[40] Depletion of the limited number of water molecules in the hydrophobic portion of the ordered lipid allows SOZ to form and accumulate in the surfactant layer.

Solvation Energy of Phospholipids and Ozonolysis Products. We observe composition changes in the lipid surfactant layer resulting from ozonolysis of saturated and unsaturated phospholipid mixtures using time-resolved FIDI-MS (Fig. 6.5 and 6.6). To understand the surface activity of phospholipids and their oxidized products, DFT calculations were performed to compute the solvation energy, ΔE_{solv}, for DPPG, POPG, and two products (carboxylate and aldehyde) from the ozonolysis of POPG. The calculated ΔE_{solv} indicates the energy difference between the gas phase and the solution phase. Lower values of ΔE_{solv} would be expected to correlate with higher surface activity of molecules at the air-liquid interface. In addition, ΔE_{solv} provides a measure of the relative hydrophobicities of similar molecules. These results provide a reasonable explanation of the observed disappearance of the ozonolysis products from the surface of the droplet over time. Calculations were performed for both neutral and anionic states of the phosphatidylglycerol group. Table 6.1 lists the calculated ΔE_{solv} values of DPPG, POPG, and the ozonolysis products of POPG. The solvation of a singly charged anion is energetically favored compared to the corresponding neutral lipid by ~ 58 kcal/mol. Both anionic and neutral DPPG and POPG exhibit similar stability in the solution phase. This supports our hypothesis, based on the observed lipid distribution in the FIDI-MS spectrum

shown in Fig. 6.5, that both DPPG and POPG are co-located at the surface of the droplet. Carboxylic acid products are more stable in the solution phase compared to intact DPPG and POPG by ~ 8 kcal/mol. Once the carboxylic acid dissolves in the solution phase, further stability can be achieved by deprotonation of carboxyl group. The ΔE_{solv} of an aldehyde product is calculated as ~ 4.5 kcal/mol less than that of an intact POPG. However, it is ~ 3.7 kcal/mol higher than the ΔE_{solv} of a carboxylic acid product. This indicates that aldehyde products have higher surface activity than carboxylic acid products at the surface of the droplet. This agrees well with the positive ion mode FIDI-MS spectra, in which aldehyde is the predominant observed product from the ozonolysis of unsaturated phospholipids (Fig.6.6).

Table 6.1 Calculated solvation energies of phospholipids and ozonolysis products

Lipid	Solvation Energy (kcal/mol)	
	Neutral	Anionic
DPPG	-32.9	-91.5[a]
POPG	-33.6	-91.7[a]
Aldehyde product	-38.3	-96.2[a]
Carboxylate product	-41.8	-100[a], -184[b]

[a]Singly charged anion with deprotonated phosphatidylglycerol group. [b]Doubly charged anion with deprotonated phosphatidylglycerol and carboxylate groups

6.3.2 Probing physical property changes by microfluidic bubble generator

Bubble Formation in a Microfluidic Device. The size of bubbles and the frequency of bubble generation were monitored to study physical characteristics induced by the change

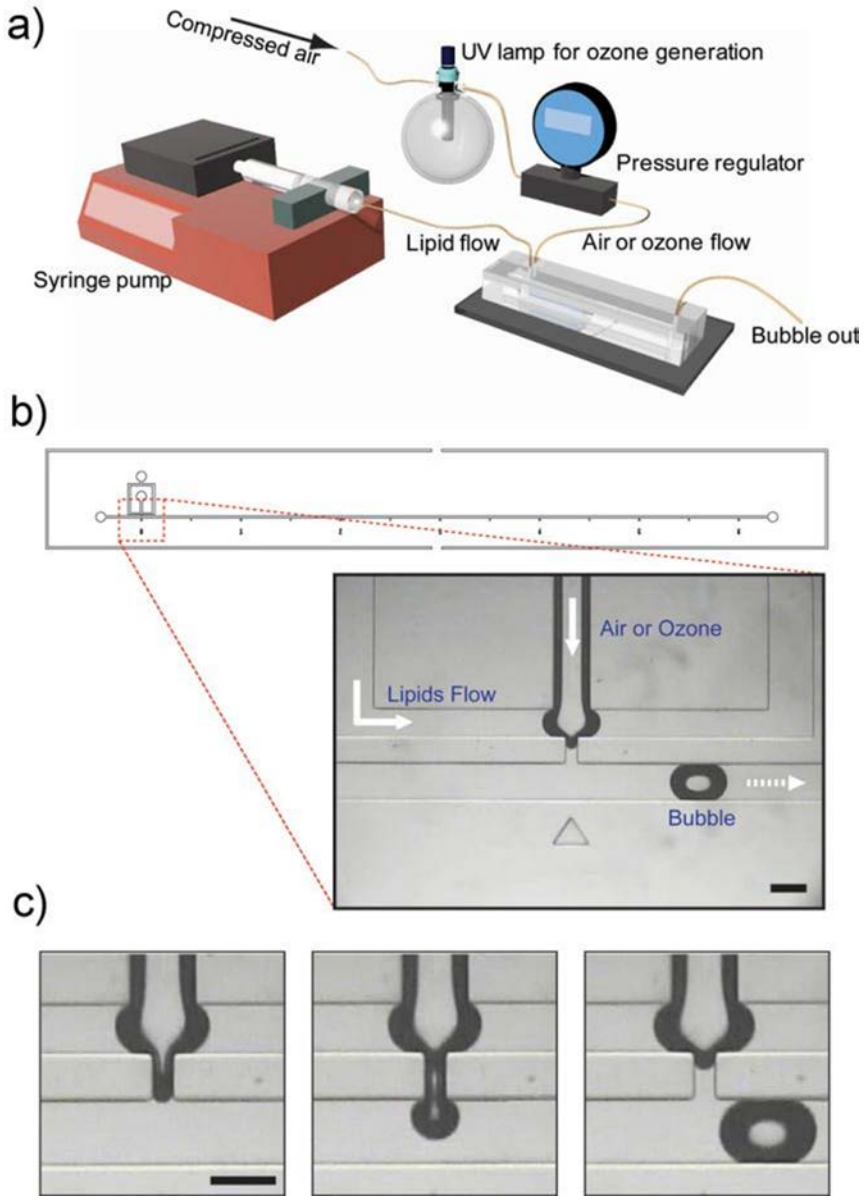

Figure 6.8 (a) Experimental setup for the bubble generation and ozone effect test. (b) Microfluidic device design for bubble generation and zoomed-in image of the bubble formation component. Air or ozone was injected from the center channel and lipid mixture was flowed from the outer two channels. The width of the narrow thread channel is 60 μm and the main flow channel for bubbles is 200 μm. (c) Representative pictures of the bubble formation process. Bubbles are generated through a pinch-off process in a reproducible manner. All scale bars: 200 μm

of chemical properties in the lipid layer. The experimental setup, device designs and bubble formation process are shown in Fig. 6.8. The bubble generation device comprises three

Table 6.2 Bubble size (in pixel) and the polydispersity index

	Air	Ozone
Average	64.43244	61.72388
Standard deviation	0.672664	1.125165
Polydispersity Index	1.043983	1.8229

$$polydispersity\ index = \frac{standard\ deviation}{average} \times 100$$

inlet channels: a center channel supplying gas and two outer channels supplying lipid mixture in solution. There is a constant inflow of lipids mixture and gas-generated bubbles in a highly reproducible manner through a pinch-off process (Fig. 6.8c). Bubbles were

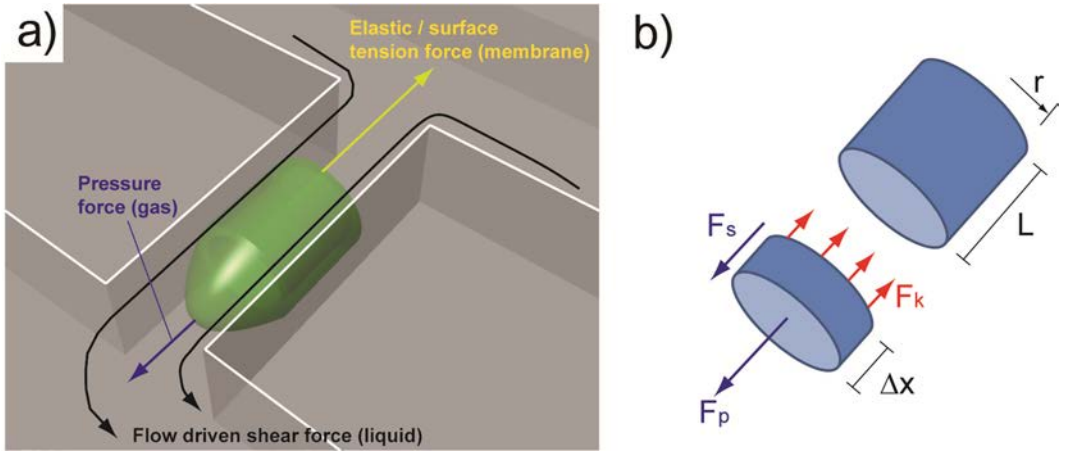

Figure 6.9 (a) Major force components for bubble generation on the lipid monolayer in the narrow channel region. Elastic force of the phospholipid monolayer at the air-liquid interface counteract the pressure force from the gas and the shear force from the bulk lipid flow. Since the pressure for the gas and the flow rate for the bulk lipid flow are fixed, the physical characteristics of the lipid monolayer plays a major role in the bubble formation process. (b) Free body diagram for the force balance. The interface in the thread (the narrow channel region) is assumed to be a cylinder.

generated with a polydispersity index of ~ 1% (Table 6.2). The polydispersity index is defined as the standard deviation of the length of the bubble divided by the mean length of the bubble in percentage. Low polydispersity index indicates that our device enables making uniform bubbles, which leads to a statistically meaningful analysis on the interface.

Most commonly used microfluidic devices for bubble generation are based on two geometries: T junction [22, 44] and FFD.[23, 34] Our design is mostly based on FFD but also has a T-junction-like characteristic due to the perpendicular main flow channel to the bubble formation components. Thus, we can think of three major factors dominant for the bubble formation: pressure force from gas, shear stress induced by flow, and the elastic property of the monolayer thin film (Fig. 6.9).[45] Since we fix the pressure of gas and the flow rate, the characteristic change in the bubble is induced by a physical property change of the lipid monolayer, such as the interfacial tension or elasticity that will be discussed below.

Ozone Effect on the Air-Liquid Interface. In previous section (6.3.1), we demonstrated the heterogeneous ozonolysis of a mixture of saturated and unsaturated phospholipids at the air-liquid interface by field-induced droplet ionization mass spectrometry (FIDI-MS).[46] We found that only the unsaturated phospholipids react with ozone and form relatively hydrophilic products such as aldehyde and carboxylic acid which dissolve into the bulk phase leaving only saturated phospholipid on the surface of the droplet at ~ 30 s of time scale. In order to visualize this chemistry in our system, we used fluorescence-labeled unsaturated lipids, NBD-PG. NBD-PG has the same structure as POPG except for the fluorescence tag on the saturated acyl chain. Constant flow of lipid mixture of DPPC, POPG, and NBD-PG was maintained and either air or ozone was

introduced to generate bubbles. Stronger fluorescence was observed at the interface near liquid phase when ozone was introduced (Fig. 6.10). The stronger fluorescence is induced by the hydrophilic products (aldehyde and carboxylate) of NBD-PG that are dissolved into the bulk phase and accumulated near the interface. This indicates that we can visually detect the chemical change of the unsaturated lipid components induced by ozonolysis, which further supports our previous finding.[46]

Since DPPC and POPG represent major components of saturated and unsaturated

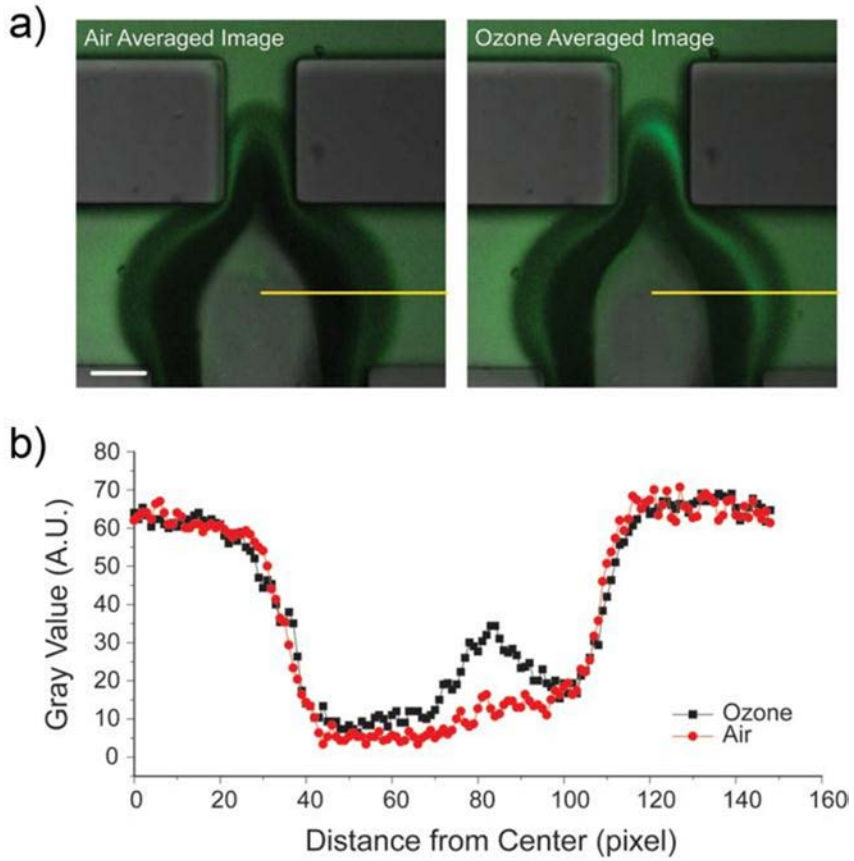

Figure 6.10 Ozone effect on the chemical composition change in the interface. (a) 10 frames averaged fluorescence images for air (left) and ozone (right) conditions. When ozone is the working gas, accumulated hydrophilic products of NBD-PG showed stronger fluorescence at the interface near bulk phase. Scale bar: 100 μm. (b) Line profile of the gray scale intensity along the yellow lines in (a). Fluorescence intensity of the ozone condition showed about a twofold increased value near the interface.

phospholipds, respectively, in our lung pulmonary surfactant system, it is interesting to see physical as well as chemical property change of the air-liquid interface induced by environmental stress such as ozone. Especially, DPPC is known as the principal phospholipid component with very low surface tension upon compression [8, 47] and POPG is known to improve the adsorption and spreading of surfactant owing to its higher fluidity.[48] Thus, dissolving POPG into the bulk solution from the interface can change the physical characteristics of the interface, which relates to lung physiology and disease. It is also notable that the increase in ozone concentration is associated with the high risk of death from respiratory causes.[4] In that sense, it is necessary to study the physical characteristics of our lung surfactant system under the environmental challenge, and microbubble can be a good model for a more in-depth understanding of the system owing to its air-liquid interface nature and similar size to the alveoli (100–300 μm).

Elastic Property of the Lipid Monolayer. We investigated the change of bubble formation processes caused by the chemical compostion alteration in a mixed lipid surfactant layer of DPPC and POPG due to the oxidative stress by ozone. In both cases, the tip of the interface near the bubble formation region oscillated significantly until the bubble was ejected to the flow (Fig. 6.11a and b). However, a significant difference was observed in a bubble formation process with ozone compared to air. In Fig. 6.11b we plotted the time-lapsed trajectories of the lower tip of the interface until bubbles were formed. Stronger oscillation was observed for the case of air compared to the case of ozone. The oscillatory characteristic indicates that the elastic property of the interface is different between air and ozone conditions. To further analyze this, we can consider the effective elastic modulus (E_{eff}) defined as

$$E_{eff} = \frac{stress}{strain}. \qquad (6.4)$$

Under the assumption that the interface near the bubble formation region (in the thread) can be simplified as a cylinder (Fig. 6.9), we can expect the following force balance at equilibrium based on the free body diagram (Fig. 6.9b),

$$F_p + F_s = F_k\,. \qquad (6.5)$$

where F_p, F_s, and F_k are pressure force, shear force and restoring elastic force, respectively. By using $F_p = p\pi r^2$ and $F_k = k\Delta x$, eq. 6.5 becomes,

$$F_s = k\Delta x - p\pi r^2. \qquad (6.6)$$

where k is the spring constant of the monolayer, Δx is tranverse displacement, p is the applied pressure, and r is the radius of the cylinder. Then,

$$E_{eff} = \frac{stress}{strain} = \frac{p + F_s/2\pi rL}{\Delta x/L}\,. \qquad (6.7)$$

where L is the initial length of the cylinder in the thread. In equilibrium condition, we can assume a harmonic oscillatory motion and the harmonic approximation leads to $F_k = k\Delta x = m(2\pi f)^2\Delta x$, where m is the mass of the oscillating body, and f is the oscillation frequency. From eqs. (6.6) and (6.7), the effective elastic modulus can be expressed as

$$E_{eff} = \frac{PL}{\Delta x}\left(1 - \frac{r}{2L}\right) + \frac{2\pi m f^2}{r}\,. \qquad (6.8)$$

Assuming that low concentration of ozone (~ 20 ppm) does not change the density of working gas, E_{eff} becomes a function of the oscillation amplitude and the frequency. Analysis on our data in Fig. 6.11b shows that E_{eff} at the interface when ozone is applied is ~ 28% higher compared to the case of air. Numerical values used for the calculation can be found in Table 6.3. As discussed earlier, once the mixture is exposed to the ozone, POPG reacts with ozone and the products dissolve into the bulk phase: This leads to the higher

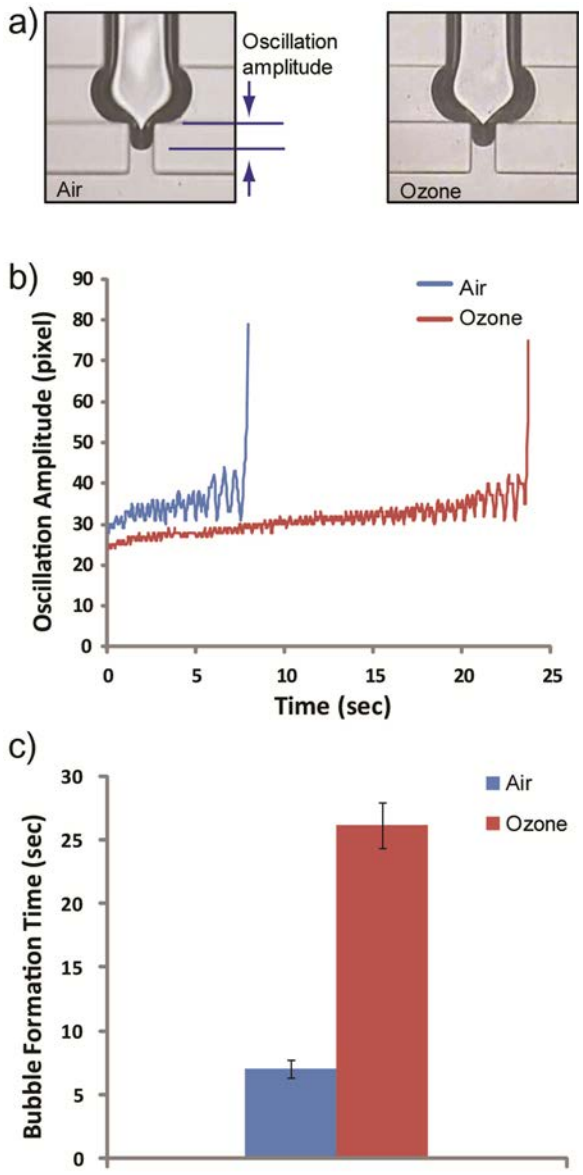

Figure 6.11 (a) Snapshots of the bubble formation component after 10 frames (0.33 s) from the previous bubble formation. (b) Time-lapsed trajectories of the lower end point of the interface. Stronger oscillation for a shorter time period was observed when air was the working gas. (c) Required time for the bubble formation

concentration of DPPC at the interfacial surfactant layer, which yields a more elastic interface (primarily due to less fluidity of the saturated lipids compared to the unsaturated ones).

Another interesting factor to look at is the time required for the bubble formation (Fig. 6.11c). Obviously longer time was required for a bubble to be generated in the ozone condition. In our cylinder-shaped harmonic oscillator model, we can use an analogy between the bubble formation process and a deformation process of a material under increasing tensile stress. Assuming that the yield strain is similar for both air and ozone cases, the longer bubble formation time (i.e., higher yield stress) means that the system is more elastic (i.e., steeper slope in the stress-strain curve). Thus, the observed longer bubble formation time when ozone is introduced also indicates the higher E_{eff} value resulted from the low POPG content at the interface.

Table 6.3 Parameters for the effective elastic modulus calculation

	Air	Ozone
p	0.42 psi	
L	75 μm	
r	30 μm	
Δx	4.575 μm	3.575 μm
f*	3.48 Hz	3.52 Hz
m	1.68×10^{-14} kg	1.31×10^{-14} kg
E_{eff}	37973.5 Pa	48595.5 Pa

* Frequency was obtained from the stable region in oscillation: for the air condition, 1.25 ~ 3.55 s and for the ozone condition, 13.75 ~ 17.30 sec regions were chosen to obtain the frequency.

Ozone Effect on Bubble Size. Bubble size is another metric for the physical property of the lipid surfactant layer. In Fig. 6.12, representative pictures of bubbles (a) and the averaged bubble sizes (b) are presented. The bubble size is smaller when ozone is the working gas. We can think of a simple scaling of the bubble size as Garstecki et al. has reported previously [34, 45] : $V_b \propto q_g \tau$, where V_b is the volume of bubble, q_g is the rate of inflow gas, and τ is the time that the thread stays open until bubble is ejected to the flow.

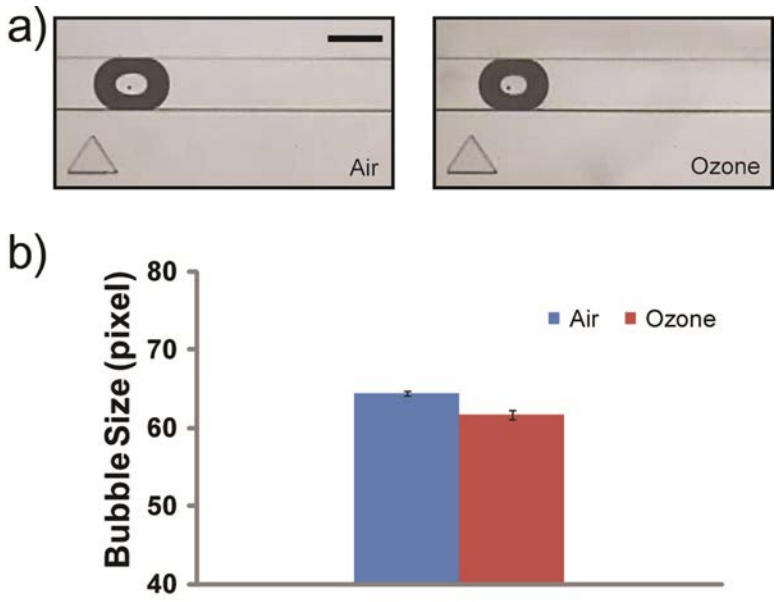

Figure 6.12 Bubble size analysis. (a) Representative images of the bubbles in different conditions. Pictures were taken when bubbles had flowed 20 mm downstream from the bubble formation component. Scale bar: 200 μm. (b) Bubble length in different conditions. The length of the bubble was measured from twenty bubbles and 10% sample trimmed mean was obtained for the analysis.

Since τ is inversely proportional to the elasticity, we can expect that high elasticity induces a shorter τ that reduces the volume of the bubble. This agrees well with our observation of increased E_{eff} and reduced size resulting from the increase of DPPC mole fraction in the surfactant layer following the heterogeneous ozonolysis of POPG. In addition to the effect of the elasticity of the surfactant layer, we can also examine the dynamic viscosity of the interface when the surfactant composition changes. The Hagen-Poiseuille relation, $q_g \propto p/\mu$ and $\tau \propto 1/q$, leads to $V_b \propto p/q\mu$, where μ is the dynamic viscosity and q is the volume flow rate of the solution. Since p and q are fixed in our experiment, we can compare the dynamic viscosity for both conditions simply by measuring bubble size. From the measured bubble scale, we found that the dynamic viscosity of the surfactant layer was increased by ~ 4.4% when ozone was used compared to pure air for bubble formation. We

found that the bubble formation process is very sensitive to the alterations of the lipid compositions in the surfactant layers and has a potential for being an analytical tool for studying interface physics.

6.4 Conclusions

The FIDI-MS technique is well suited to analyze chemical reactions of phospholipids at the air-liquid interface. In FIDI-MS spectra, ozonolysis products distinct from those formed in both the bulk-phase and the gas-phase are observed from an interfacial phospholipid surfactant layer. MD simulations correlate well with experimental observations and provide additional insights into the interactions between lipids and water molecules in the interfacial region. In these simulations the low water density around unsaturated carbons of the lipid acyl chain provides a rationalization for the experimental observation of metastable products resulting from ozonolysis of unsaturated phospholipids.

In the lung, oxidation of pulmonary surfactant causes surfactant dysfunction in adsorption and respreading process, as well as reduction of surface tension.[49, 50] Once O_3 traverses the air-liquid interface, it decays rapidly concomitant with the formation of ROS in regions with high water densities.[51] However, due to the high reactivity with PS at the interface, it has been thought that little or none of the O_3 can penetrate the PS monolayer to attack the epithelium cells below.[52] Instead of direct attack by O_3 and its derivative ROS, secondary oxidized products of PS, such as HHP, have been expected to yield cellular damage.[52] Our FIDI-MS data indicate that more than 60% of the heterogeneous oxidation products of POPG by O_3 are peroxides. These products, which are more water soluble than

the lipid precursors, eventually dissolve into the bulk liquid where they form ROS[36] that can lead to cellular damage.

These findings provide mechanistic details for the reaction of ozone with unsaturated phospholipids, leading to possible damage of the pulmonary system by ROS or direct ozone exposure. Further studies with more elaborate model systems comprising surfactant proteins and various lipids could further clarify the effect of environmental exposures on the lung surfactant system. We have reported one such study, demonstrating that phospholipid surfactants have a profound effect in moderating the reactions of the important surfactant protein B with ozone.[19]

We also have developed a microfluidic bubble generator that enables the analysis of physical property changes in a model pulmonary surfactant layer at the air-liquid interface under oxidative stress condition. The bubble formation process was very sensitive to the surfactant composition. Chemical composition change of the phospholipid mixture under oxidative stress in the air-liquid interface was identified visually through fluorescence monitoring. Our platform was further validated for its potential use in studying the physical characteristics of the interface resulting from chemical reactions at the interface. Heterogeneous reactions followed by chemical composition changes have been studied as important parameters on the physics of the lipid surfactant, and we were able to observe their effects in terms of the bubble size and the formation process, especially oscillatory behavior. Owing to the sensitive response, reproducibility for good statistics, and the ease of manipulation/analysis, we believe that microbubbles in microfluidics have potential in understanding the interfacial physics as well as chemistry of the various surfactant systems.

6.5 References

1. Stansfield, A. D.; Jump, Z.; Sodlosky, S.; Rappaport, S.; Edelman, N.; Haldorsen, J.; Javed, T.; Martin, C.; Margulies, E. *Lung disease data: 2008*; American Lung Association National Headquarters. New York, 2008.
2. Anseth, J. W.; Goffin, A. J.; Fuller, G. G.; Ghio, A. J.; Kao, P. N.; Upadhyay, D., Lung surfactant gelation induced by epithelial cells exposed to air pollution or oxidative stress. *American Journal of Respiratory Cell and Molecular Biology* **2005,** 33, (2), 161–168.
3. Halliwell, B.; Gutteridge, J. M. C., Oxygen-toxicity, oxygen radicals, transition-metals and disease. *Biochemical Journal* **1984,** 219, (1), 1–14.
4. Jerrett, M.; Burnett, R. T.; Pope, C. A.; Ito, K.; Thurston, G.; Krewski, D.; Shi, Y. L.; Calle, E.; Thun, M., Long-Term Ozone Exposure and Mortality. *New England Journal of Medicine* **2009,** 360, (11), 1085–1095.
5. Perez-Gil, J.; Keough, K. M. W., Interfacial properties of surfactant proteins. *Biochimica Et Biophysica Acta—Molecular Basis of Disease* **1998,** 1408, (2–3), 203–217.
6. Lambert, M. G.; Vangolde, L. M. G.; Batenburg, J. J.; Robertson, B., The pulmonary surfactant system–biochemical aspects and functional significance. *Physiological Reviews* **1988,** 68, (2), 374–455.
7. Schram, V.; Hall, S. B., SP-13 and SP-C alter diffusion in Bilayers of pulmonary surfactant. *Biophysical Journal* **2004,** 86, (6), 3734-3743.

8. Hawco, M. W.; Davis, P. J.; Keough, K. M. W., Lipid Fluidity in Lung Surfactant—Monolayers of Saturated and Unsaturated Lecithins. *Journal of Applied Physiology* **1981,** 51, (2), 509–515.
9. Diemel, R. V.; Snel, M. M. E.; Waring, A. J.; Walther, F. J.; van Golde, L. M. G.; Putz, G.; Haagsman, H. P.; Batenburg, J. J., Multilayer formation upon compression of surfactant monolayers depends on protein concentration as well as lipid composition—An atomic force microscopy study. *Journal of Biological Chemistry* **2002,** 277, (24), 21179-21188.
10. Perez-Gil, J., Molecular interactions in pulmonary surfactant films. *Biology of the Neonate* **2002,** 81, 6–15.
11. Grimm, R. L.; Hodyss, R.; Beauchamp, J. L., Probing interfacial chemistry of single droplets with field-induced droplet ionization mass spectrometry: Physical adsorption of polycyclic aromatic hydrocarbons and ozonolysis of oleic acid and related compounds. *Analytical Chemistry* **2006,** 78, (11), 3800–3806.
12. Voss, L. F.; Hadad, C. M.; Allen, H. C., Competition between atmospherically relevant fatty acid monolayers at the air/water interface. *Journal of Physical Chemistry B* **2006,** 110, (39), 19487–19490.
13. Mundy, C. J.; Kuo, I. F. W., First-principles approaches to the structure and reactivity of atmospherically relevant aqueous interfaces. *Chemical Reviews* **2006,** 106, (4), 1282–1304.
14. Gonzalez-Labrada, E.; Schmidt, R.; DeWolf, C. E., Kinetic analysis of the ozone processing of an unsaturated organic monolayer as a model of an aerosol surface. *Physical Chemistry Chemical Physics* **2007,** 9, (43), 5814–5821.

15. Enami, S.; Hoffmann, M. R.; Colussi, A. J., Acidity enhances the formation of a persistent ozonide at aqueous ascorbate/ozone gas interfaces. *Proceedings of the National Academy of Sciences of the United States of America* **2008,** 105, (21), 7365–7369.

16. Enami, S.; Hoffmann, M. R.; Colussi, A. J., Ozonolysis of uric acid at the air/water interface. *Journal of Physical Chemistry B* **2008,** 112, (14), 4153–4156.

17. Grimm, R. L.; Beauchamp, J. L., Field-induced droplet ionization mass spectrometry. *Journal of Physical Chemistry B* **2003,** 107, (51), 14161–14163.

18. Grimm, R. L.; Beauchamp, J. L., Dynamics of field-induced droplet ionization: Time-resolved studies of distortion, jetting, and progeny formation from charged and neutral methanol droplets exposed to strong electric fields. *Journal of Physical Chemistry B* **2005,** 109, (16), 8244–8250.

19. Kim, H. I.; Kim, H. J.; Shin, Y. S.; Beegle, L. W.; Jang, S. S.; Neidholdt, E. L.; Goddard, W. A.; Heath, J. R.; Kanik, I.; Beauchamp, J. L., Interfacial Reactions of Ozone with Surfactant Protein B in a Model Lung Surfactant System. *Journal of the American Chemical Society* **2010,** 132, (7), 2254–2263.

20. Hashimoto, M.; Shevkoplyas, S. S.; Zasonska, B.; Szymborski, T.; Garstecki, P.; Whitesides, G. M., Formation of Bubbles and Droplets in Parallel, Coupled Flow-Focusing Geometries. *Small* **2008,** 4, (10), 1795–1805.

21. Garstecki, P.; Fuerstman, M. J.; Whitesides, G. M., Oscillations with uniquely long periods in a microfluidic bubble generator. *Nature Physics* **2005,** 1, (3), 168–171.

22. Garstecki, P.; Fuerstman, M. J.; Stone, H. A.; Whitesides, G. M., Formation of droplets and bubbles in a microfluidic T-junction-scaling and mechanism of break-up. *Lab on a Chip* **2006,** 6, (3), 437–446.

23. Anna, S. L.; Bontoux, N.; Stone, H. A., Formation of dispersions using "flow focusing" in microchannels. *Applied Physics Letters* **2003,** 82, (3), 364–366.

24. Prakash, M.; Gershenfeld, N., Microfluidic bubble logic. *Science* **2007,** 315, (5813), 832–835.

25. Weis, M.; Kopani, M.; Jakubovsky, J.; Danihel, L., Ethanol and methanol induced changes in phospholipid monolayer. *Applied Surface Science* **2006,** 253, (5), 2425–2431.

26. MacKerell, A. D.; Bashford, D.; Bellott, M.; Dunbrack, R. L.; Evanseck, J. D.; Field, M. J.; Fischer, S.; Gao, J.; Guo, H.; Ha, S.; Joseph-McCarthy, D.; Kuchnir, L.; Kuczera, K.; Lau, F. T. K.; Mattos, C.; Michnick, S.; Ngo, T.; Nguyen, D. T.; Prodhom, B.; Reiher, W. E.; Roux, B.; Schlenkrich, M.; Smith, J. C.; Stote, R.; Straub, J.; Watanabe, M.; Wiorkiewicz-Kuczera, J.; Yin, D.; Karplus, M., All-atom empirical potential for molecular modeling and dynamics studies of proteins. *Journal of Physical Chemistry B* **1998,** 102, (18), 3586–3616.

27. Plimpton, S., Fast Parallel Algorithms for Short-range Molecular-Dynamics. *Journal of Computational Physics* **1995,** 117, (1), 1–19.

28. Hockney, R. W.; Eastwood, J. W., *Computer simulation using particles*. McGraw-Hill: New York, 1981.

29. Tannor, D. J.; Marten, B.; Murphy, R.; Friesner, R. A.; Sitkoff, D.; Nicholls, A.; Ringnalda, M.; Goddard, W. A.; Honig, B., Accurate First Principles Calculation of Molecular Charge-distributions and Solvation Energies from Ab-Initio Quantum-

Mechanics and Continuum Dielectric Theory. *Journal of the American Chemical Society* **1994,** 116, (26), 11875–11882.

30. Marten, B.; Kim, K.; Cortis, C.; Friesner, R. A.; Murphy, R. B.; Ringnalda, M. N.; Sitkoff, D.; Honig, B., New model for calculation of solvation free energies: Correction of self-consistent reaction field continuum dielectric theory for short-range hydrogen-bonding effects. *Journal of Physical Chemistry* **1996,** 100, (28), 11775–11788.
31. Becke, A. D., Density-Functional Thermochemistry .3. the Role of Exact Exchange. *Journal of Chemical Physics* **1993,** 98, (7), 5648–5652.
32. Lee, C. T.; Yang, W. T.; Parr, R. G., Development of the Colle-Salvetti Correlation-Energy Formula into a Functional of the Electron-Density. *Physical Review B* **1988,** 37, (2), 785–789.
33. Duffy, D. C.; McDonald, J. C.; Schueller, O. J. A.; Whitesides, G. M., Rapid Prototyping of Microfluidic Systems in Poly(dimethylsiloxane). *Analytical Chemistry* **1998,** 70, (23), 4974–4984.
34. Garstecki, P.; Gitlin, I.; DiLuzio, W.; Whitesides, G. M.; Kumacheva, E.; Stone, H. A., Formation of monodisperse bubbles in a microfluidic flow-focusing device. *Applied Physics Letters* **2004,** 85, (13), 2649–2651.
35. Karagulian, F.; Lea, A. S.; Dilbeck, C. W.; Finlayson-Pitts, B. J., A new mechanism for ozonolysis of unsaturated organics on solids: phosphocholines on NaCl as a model for sea salt particles. *Physical Chemistry Chemical Physics* **2008,** 10, (4), 528–541.
36. Santrock, J.; Gorski, R. A.; Ogara, J. F., Products and Mechanism of the Reaction of Ozone with Phospholipids in Unilamellar Phospholipid-Vesicles. *Chemical Research in Toxicology* **1992,** 5, (1), 134–141.

37. Rivera, J. L.; Starr, F. W.; Paricaud, P.; Cummings, P. T., Polarizable contributions to the surface tension of liquid water. *Journal of Chemical Physics* **2006,** 125, (9), 8.

38. Ghosh, A.; Smits, M.; Bredenbeck, J.; Bonn, M., Membrane-bound water is energetically decoupled from nearby bulk water: An ultrafast surface-specific investigation. *Journal of the American Chemical Society* **2007,** 129, (31), 9608–9609.

39. Lai, C. C.; Yang, S. H.; Finlaysonpitts, B. J., Interactions of Monolayers of Unsaturated Phosphocholines with Ozone at the Air-Water-Interface. *Langmuir* **1994,** 10, (12), 4637–4644.

40. Pryor, W. A., Can Vitamin-E Protect Humans Against the Pathological Effects of Ozone in Smog. *American Journal of Clinical Nutrition* **1991,** 53, (3), 702–722.

41. Kaznessis, Y. N.; Kim, S. T.; Larson, R. G., Simulations of zwitterionic and anionic phospholipid monolayers. *Biophysical Journal* **2002,** 82, (4), 1731–1742.

42. Kaznessis, Y. N.; Kim, S.; Larson, R. G., Specific mode of interaction between components of model pulmonary surfactants using computer simulations. *Journal of Molecular Biology* **2002,** 322, (3), 569–582.

43. Baoukina, S.; Monticelli, L.; Risselada, H. J.; Marrink, S. J.; Tieleman, D. P., The molecular mechanism of lipid monolayer collapse. *Proceedings of the National Academy of Sciences of the United States of America* **2008,** 105, (31), 10803–10808.

44. Thorsen, T.; Roberts, R. W.; Arnold, F. H.; Quake, S. R., Dynamic pattern formation in a vesicle-generating microfluidic device. *Physical Review Letters* **2001,** 86, (18), 4163–4166.

45. Garstecki, P.; Stone, H. A.; Whitesides, G. M., Mechanism for flow-rate controlled breakup in confined geometries: a route to monodisperse emulsions. *Physical Review Letters* **2005,** 94, (16), 164501.

46. Kim, H. I.; Kim, H.; Shin, Y. S.; Beegle, L. W.; Goddard, W. A.; Heath, J. R.; Kanik, I.; Beauchamp, J. L., Time Resolved Studies of Interfacial Reactions of Ozone with Pulmonary Phospholipid Surfactants Using Field Induced Droplet Ionization Mass Spectrometry. *The Journal of Physical Chemistry B* **2010,** 114, (29), 9496–9503.

47. Wang, Z. D.; Hall, S. B.; Notter, R. H., Dynamic Surface-Activity of Films of Lung Surfactant Phospholipids, Hydrophobic Proteins, and Neutral Lipids. *Journal of Lipid Research* **1995,** 36, (6), 1283–1293.

48. Gopal, A.; Lee, K. Y. C., Morphology and collapse transitions in binary phospholipid monolayers. *Journal of Physical Chemistry B* **2001,** 105, (42), 10348–10354.

49. Gilliard, N.; Heldt, G. P.; Loredo, J.; Gasser, H.; Redl, H.; Merritt, T. A.; Spragg, R. G., Exposure of the Hydrophobic Components of Porcine Lung Surfactant to Oxidant Stress Alters Surface-Tension Properties. *Journal of Clinical Investigation* **1994,** 93, (6), 2608–2615.

50. Rodriguez-Capote, K.; Manzanares, D.; Haines, T.; Possmayer, F., Reactive oxygen species inactivation of surfactant involves structural and functional alterations to surfactant proteins SP-B and SP-C. *Biophysical Journal* **2006,** 90, (8), 2808–2821.

51. von Gunten, U., Ozonation of drinking water: Part I. Oxidation kinetics and product formation. *Water Research* **2003,** 37, (7), 1443–1467.

52. Pryor, W. A., How Far Does Ozone Penetrate into the Pulmonary Air Tissue Boundary Before It Reacts. *Free Radical Biology and Medicine* **1992,** 12, (1), 83–88.